J. Phycol. **49,** 401–416 (2013)
© 2013 Phycological Society of America
DOI: 10.1111/jpy.12051

POLYPHASIC EVALUATION OF *XANTHIDIUM ANTILOPAEUM* AND *XANTHIDIUM CRISTATUM* (ZYGNEMATOPHYCEAE, STREPTOPHYTA) SPECIES COMPLEX[1]

Jan Stastny,[2] *Pavel Skaloud*

Department of Botany, Faculty of Science, Charles University in Prague, Benátská 2, Prague, CZ-12801, Czech Republic

Dorothee Langenbach

Botanisches Institut, Lehrstuhl I, Universität zu Köln, Zülpicherstr. 47b, Köln, D-50674, Germany

Katarina Nemjova and Jiri Neustupa

Department of Botany, Faculty of Science, Charles University in Prague, Benátská 2, Prague, CZ-12801, Czech Republic

We investigated twenty-six strains of *Xanthidium antilopaeum* Kütz. and seven strains of *X. cristatum* Ralfs isolated from various European localities or obtained from public culture collections. A combination of molecular, geometric morphometric, and morphological data were used to reveal the patterns of the phylogenetic and morphological differentiation of these taxonomically very complicated desmid taxa. The molecular data based on *trn*G^{ucc} and ITS rDNA sequences illustrated the monophyly of both the complexes, which indicated that their traditional morphology-based discriminative criteria, such as the different number of spines, may generally continue to be considered relevant. The single exception was *X. antilopaeum* var. *basiornatum* B. Eichler et Raciborski, which was positioned outside the *X. antilopaeum/cristatum* clade. The independent status of this taxon was also confirmed on the basis of the geometric morphometric data, so that we concluded that it probably represents a separate species. Within *X. cristatum* complex, the traditional varieties *X. cristatum* var. *cristatum* Ralfs, *X. cristatum* var. *uncinatum* Ralfs, and *X. cristatum* var. *scrobiculatum* Scott et Grönblad turned out to be separate taxa. Conversely, *X. cristatum* var. *bituberculatum* Lowe lacked any taxonomical value. Our data on *X. antilopaeum* illustrated extensive phylogenetic as well as phenotypic variability within this species complex. However, our data did not result in any unambiguous pattern that would allow sound taxonomic classification. Finally, we also found out that the morphologically peculiar *Staurastrum tumidum* Ralfs belongs to the genus *Xanthidium* based on the combined *rbc*L + *cox* III data set. Consequently, this species was formally transferred to this genus.

Key index words: **Desmidiales; geometric morphometrics; molecular phylogeny; taxonomy; *Xanthidium***

Desmids belong to the Zygnematophyceae, the largest and the most diverse group of streptophyte green algae (Gontcharov and Melkonian 2005). They are known for their high morphological variation that led to the description of over 4,000 species (Gontcharov et al. 2003, Gontcharov 2008). As inhabitants of freshwater wetlands, desmids belong to the most important phytobenthic groups in these habitats, in terms of both species richness and biomass (Coesel and Meesters 2007). Therefore, they have been frequently used in various kinds of ecological and biomonitoring studies (Coesel 2001, 2003, Pals et al. 2006, Krasznai et al. 2008, Neustupa et al. 2009, 2011a). Their suitability and reliability for these purposes essentially requires reliable species concepts. However, the traditional desmid taxonomy, based entirely on morphological features, has recently been challenged by molecular data. Molecular research has increasingly, and sometimes controversially, been turning desmid taxonomy upside down, especially at the generic level (McCourt et al. 2000, Gontcharov et al. 2003, Gontcharov and Melkonian 2005, 2008, 2010, 2011, Gontcharov 2008, Hall et al. 2008, Škaloud et al. 2011). Most of the traditional species-rich genera were found to be polyphyletic or paraphyletic (Gontcharov and Melkonian 2005, 2008, Gontcharov 2008). However, while we now know that most of the traditional generic concepts have been inadequate, little information is available on the validity of traditional desmidiacean species concepts. In many desmids, the extensive morphological variation within the range of traditionally defined species led to the descriptions of numerous infraspecific taxa, whose taxonomic validity remained largely unresolved (Kouwets 2008). Several studies based on crossbreeding experiments (Blackburn and Tyler 1987, Denboh et al. 2003) indicated that concepts of at least some desmid species have been too broad, implicating some degree of pseudocryptic or cryptic species diversity. This opinion has been further supported by several recent studies that used a combination of molecular, morphological, and

[1]Received 9 August 2012. Accepted 6 November 2012.
[2]Author for correspondence: e-mail stastny.jan@centrum.cz.

geometric morphometric methods that revealed surprising microevolutionary differentiation within several desmid species. The studies on *Micrasterias crux-melitensis/M. radians* (Neustupa et al. 2010) and *M. truncata* complexes (Nemjová et al. 2011) illustrated pseudocryptic diversity within these traditional desmid taxa. Several morphologically defined infraspecific taxa were shown to be artificial and probably lacking any taxonomic value, but some of the other varieties apparently represented independent species. Another study that focused on the *M. rotata/M. fimbriata* species complex (Neustupa et al. 2011b) revealed phylogenetic homogeneity of traditional *M. rotata* but it also illustrated that European populations of *M. fimbriata* actually belong to two species lineages. It has to be noted that in the above-mentioned studies, individual species-level phylogenetic lineages were always found to be morphologically perfectly identifiable, both by careful microscopic analysis, as well as by geometric morphometrics. However, these studies comprised only the representatives of the morphologically most conspicuous genus *Micrasterias*, while there are still no phylogenetic data on the validity of traditional species concepts in other desmidiacean genera, often disposing much less morphological discriminative characters than the above-mentioned genus.

The genus *Xanthidium* Ralfs is a widely distributed, well-known desmid genus with more than 110 morphologically delimited species (Gontcharov and Melkonian 2011). It was characterized by biradiate cells with multiform semicells, provided with a series of spines usually confined to the semicell angles (Coesel and Meesters 2007). The type species of the genus *Xanthidium* has not yet been designated (Guiry and Guiry 2012). The genus as a whole was found to be polyphyletic on the basis of molecular phylogenetic analysis (Gontcharov and Melkonian 2011). However, several of the traditional "core" *Xanthidium* species, such as *Xanthidium antilopaeum*, *X. cristatum*, *X. subhastiferum*, and *X. brebissonii*, were recovered in a single well-supported phylogenetic lineage within Desmidiaceae (Gontcharov and Melkonian 2011). Conversely, *X. octocorne* Ralfs was found to be part of a strongly supported *Staurodesmus* lineage (Gontcharov and Melkonian 2011). Conversely, Gontcharov et al. (2003) and Gontcharov and Melkonian (2011) illustrated a possible sister relationship of *Staurastrum tumidum* Ralfs to the "core" *Xanthidium* lineage.

In the present study, we evaluated the phylogenetic and morphological patterns in the well-known traditional species *X. antilopaeum* Kütz. and *X. cristatum* Ralfs. These species belong to one of the most frequently occurring representatives of the genus, and *X. antilopaeum* has even been considered to be one of the most frequently occurring desmids in the temperate European peatlands (Lenzenweger 1997). According to the traditional morphological criteria, *X. cristatum* can be distinguished from *X. antilopaeum* by the different number of cellular spines, possessing a total of 10 instead of eight spines per semicell that are typically present in *X. antilopaeum* (West and West 1912). Both taxa, however, exhibit notable morphological variation that led to the taxonomic description of numerous infraspecific taxa, differing in the arrangement of the marginal spines and the central pattern of scrobiculae (Coesel and Meesters 2007). In total, 93 infraspecific taxa have been described in *X. antilopaeum* and 42 in *X. cristatum* (Guiry and Guiry 2012). Many of these traditional subspecific taxa may have no phylogenetic value, and *X. antilopaeum* and *X. cristatum* have therefore been considered to belong to the taxonomically most problematic desmids (Prescott et al. 1982). Coesel (2005) suggested that some of the *X. antilopaeum* varieties are so different from the nominate variety that they might be considered species of their own. Therefore, we focused on infraspecific variation within these two morphologically very diverse species. In total, we examined 26 strains of *X. antilopaeum* and 7 strains of *X. cristatum*. The strains were isolated from natural samples obtained from across Europe, or they had been obtained from public culture collections. Morphology of the strains was ascertained, and, if possible, they were identified to the variety level. In addition, morphological diversity of strains was assessed by geometric morphometrics and by performing scanning electron microscopy (SEM). Geometric morphometrics is a quantitative method for the evaluation of biological shapes that has recently been used for the morphological variation analyses in various groups of microalgae (e.g., Beszteri et al. 2005, Potapova and Hamilton 2007, Veselá et al. 2009), including desmids (Neustupa and Šťastný 2006, Neustupa et al. 2010, 2011b, Nemjová et al. 2011). SEM has also been considered to be a key additional tool for the examination of the richly sculptured cell wall of desmids (Coesel 1984, Gontcharov et al. 2002). The gene sequence data of four molecular markers (ITS rDNA, *cox*III, *rbc*L, and *trn*G^{ucc}) were analyzed to evaluate the phylogenetic position of strains and to test for the monophyly and phylogenetic differentiation of the two investigated traditional species.

In summary, we primarily asked whether *X. antilopaeum* and *X. cristatum* consist of phylogenetically homogenous entities, i.e., whether the traditional morphology-based discriminative characters (the different number of spines per semicell) may still be considered to be relevant. Moreover, we aimed to resolve the inner phylogenetical structure within both complexes, and we attempted to identify morphological peculiarities of the newly recognized species-level lineages. Finally, we intended to corroborate the unusual phylogenetic position of *S. tumidum* by sequencing our own isolate of this species.

MATERIALS AND METHODS

Isolation and cultivation of strains and LM and SEM observations. For this study, we isolated 21 strains of *X. antilopaeum* and *X. cristatum* and 1 strain of *S. tumidum* from various European wetlands (Table 1). In addition, 12 strains of *X. antilopaeum* and *X. cristatum* were obtained from public culture collections such as Sammlung von Conjugaten-Kulturen, University Hamburg (SVCK) and Culture Collection of Algae, University of Vienna (ASW), nowadays deposited in the Culture Collection of Algae at the University of Cologne (CCAC; Table 1). The clonal strains were isolated by single-cell

TABLE 1. Origin and description of strains.

Strain no.	Taxon name	Origin	Geographic coordinates
H 21	*Xanthidium antilopaeum* var. *antilopaeum*	Grand Étang de Biscarosse, Aquitaine, France	44°23′13.60″N, 1°11′18.90″W
H 23	*Xanthidium antilopaeum* var. *antilopaeum*	Huťský pond, Czech Republic	48°39′20.99″ N, 14°40′56.36″ E
H 25	*Xanthidium antilopaeum* var. *antilopaeum*	Étang de Cazaux, Aquitaine, France	44°30′39.20″N, 1°11′25.15″W
H 27	*Xanthidium antilopaeum* var. *antilopaeum*	Borkovická blata peat bog, Czech Republic	49°14′9.36″ N, 14°37′24.84″ E
H 29	*Xanthidium antilopaeum* var. *antilopaeum*	Pískovny Cep I sandpits, Czech Republic	48°55′6.119″N, 14°53′3.058″E
H 31	*Xanthidium antilopaeum* var. *antilopaeum*	Pískovny Cep I sandpits, Czech Republic	48°55′6.119″N, 14°53′3.058″E
H 32	*Xanthidium antilopaeum* var. *antilopaeum*	Bastemose, Bornholm, Denmark	55°07′37.63″N, 14°56′42.15″E
SVCK 28	*Xanthidium antilopaeum* var. *antilopaeum*	Fischteiche-Wolkersdorf near Frankenberg, Germany	—
SVCK 281	*Xanthidium antilopaeum* sensu lato	Burnham's Swamp near Falmouth, USA	—
SVCK 343	*Xanthidium antilopaeum* sensu lato	Pitztal, Austria	—
SVCK 105	*Xanthidium antilopaeum* sensu lato	Fokstumyr northeast from Dombas, Norway	62°07′18.49″N, 9°15′32.27″E
ASW 07105	*Xanthidium antilopaeum* sensu lato	Reservoir for drinking water, Jakobshaven, Greenland	—
ASW 07106	*Xanthidium antilopaeum* sensu lato	Reservoir for drinking water, Jakobshaven, Greenland	—
ASW 07107	*Xanthidium antilopaeum* sensu lato	Pool in the tundra, St. Matthew Island, Bering Sea, USA	—
H 26	*Xanthidium antilopaeum* sensu lato	A peaty pool near Maumwee Lough, Ireland	53°28′27.30″N, 9°32′38.52″W
H 17	*Xanthidium antilopaeum* var. *basiornatum*	Schwemm near Walchsee peat bog, Austria	47°39′34.52″N, 12°17′50.51″E
H 22	*Xanthidium antilopaeum* var. *depauperatum*	Eirk Lough, Kerry, Ireland	51°56′25.36″N, 9°37′37.85″W
H 20	*Xanthidium antilopaeum* var. *laeve*	A peaty pool near Maumwee Lough, Ireland	53°28′27.30″N, 9°32′38.52″W
SVCK 147	*Xanthidium antilopaeum* var. *minneapoliense*	A pool northeast from Raleigh, USA	—
H 30	*Xanthidium antilopaeum* var. *polymazum*	An unnamed lake, Connemara, Ireland	53°34′10.60″N, 9°48′29.57″W
H 10	*Xanthidium antilopaeum* var. *incrassatum*	Břehyně wetland, Czech Republic	50°34′59.72″N, 14°42′17.76″E
H 19	*Xanthidium antilopaeum* var. *incrassatum*	Schwemm near Walchsee peat bog, Austria	47°39′34.52″N, 12°17′50.51″E
H 15	*Xanthidium antilopaeum* var. *planum*	Marienteich, Czech Republic	50°32′43.53″N, 14°40′39.44″E
H 18	*Xanthidium antilopaeum* var. *planum*	Schwemm near Walchsee peat bog, Austria	47°39′34.52″N, 12°17′50.51″E
H 28	*Xanthidium antilopaeum* var. *planum*	An unnamed lake near Upper Lake, Kerry, Ireland	51°57′57.66″N 9°35′49.24″W
SVCK 74	*Xanthidium antilopaeum* var. *planum*	Peaty pool south from Koli, Finland	—
H 59	*Xanthidium cristatum* var. *cristatum*	Mariánský pond, Czech Republic	50°32′43.53″N, 14°40′39.44″E
ASW 07060	*Xanthidium cristatum* var. *cristatum*	An unnamed bog, Finland	—
ASW 07101	*Xanthidium cristatum* var. *cristatum*	A peat bog near Tamsweg, Salzburg, Austria	—
H 08	*Xanthidium cristatum* var. *scrobiculatum*	The Long Range, Kerry, Ireland	51°59′51.04″N, 9°33′3.81″W
H 11	*Xanthidium cristatum* var. *scrobiculatum*	An unnamed lake, Connemara, Ireland	53°34′10.60″N, 9°48′29.57″W
ASW 07102	*Xanthidium cristatum* var. *scrobiculatum*	Skarsvag, Norway	—
H 12	*Xanthidium cristatum* var. *uncinatum*	Břehyně wetland, Czech Republic	50°35′4.27″N, 14°42′24.95″E
H 76	*Staurastrum tumidum*	Dvořiště peat bog, Czech Republic	49°4′14.09″N, 14°38′59.31″E

pipetting. To achieve relatively rapid growth of the strains, they were cultured in the MES-buffered DY IV liquid medium at 24°C and continuously illuminated at 5–15 μmol photons $\cdot m^{-2} \cdot s^{-1}$ from 18 W cool fluorescent tubes (Philips TLD 18W/33, Royal Philips Electronics, Amsterdam, Netherlands). Microphotographs of the cells were obtained using an Olympus BX51 (Olympus, Tokyo, Japan) light microscope with an Olympus Z5060 digital camera. For SEM, the acetone-washed glass coverslips were heated, and coated three times with a poly-L-lysine solution (1:10 in deionized water) to ensure appropriate cell adhesion. A drop of the formaldehyde-fixed cell suspension was transferred into 30% acetone, and dehydrated by using an acetone series. Subsequently, the cells were dried to a critical point by using liquid CO_2. Finally, they were sputter coated with gold (Bal-Tec Sputter Coater SCD 050, Capovani Brothers Inc., Sconia, NY, USA) and examined using a JEOL 6380 LV (JEOL Ltd., Tokyo, Japan) scanning electron microscope.

DNA isolation, amplification, and sequencing. After centrifugation of desmid cells in 2 mL tubes, 100–200 mL of the InstaGene matrix (Bio-Rad Laboratories, Hercules, CA, USA) was added to the pellet. Then, the cells were mechanically disrupted by shaking for 5 min with glass beads (3 mm in diameter; Sigma-Aldrich, St. Louis, MO, USA) in Mixer Mill MM 400 (RETSCH GmbH, Haan, Germany). Subsequently, the solution was incubated at 56°C for 30 min, vortexed for 10 s, and heated at 99°C for 8 min. After another vortexing step, the tubes were centrifuged at 16,000 rcf for 2 min. Finally, the supernatant (DNA) was diluted to a concentration of 10 ng $\cdot \mu L^{-1}$ for use in polymerase chain reaction (PCR) amplification. Four molecular markers were amplified by PCR: chloroplast *rbc*L and *trn*G^{ucc}, mitochondrial *cox*III, and nuclear ITS rDNA. The PCR reaction in total volume of 20 μL contained 13.1 μL of sterile Mili-Q water, 2 μL of AmpliTaq Gold® 360 Buffer 10 × (Applied Biosystems, Life technologies, Carlsbad, CA, USA), 2.2 μL of $MgCl_2$ (25 mM), 0.4 μL of dNTP mix (10 mM), 0.25 μL of each primer (25 nM), 0.6 μL of 360 GC enhancer, 0.2 μL of AmpliTaq Gold® 360 DNA Polymerase, and 1 μL of DNA (10 ng $\cdot \mu L^{-1}$). The PCR amplification was performed in either a Touchgene Gradient Thermal Cycler (Krackeler Scientific, Albany, NY, USA) or an XP thermal cycler (Bioer, Tokyo, Japan). Amplification primers and cycling conditions are listed in Table 2 and Table 3. The PCR products were stained using bromophenol blue loading dye, quantified on 1% agarose gel, stained with ethidium bromide, and cleaned with the JETQUICK PCR Purification Kit (Genomed, Löhne, Germany), according to the manufacturer's protocol. The purified amplification products were sequenced using an Applied Biosystems (Seoul, Korea) automated sequencer (ABI 3730 × l) at Macrogen Corp. in Seoul, Korea. The sequencing reads were assembled and edited using the SeqAssem programme (Hepperle 2004).

Sequence alignment. Three different alignments were constructed for the phylogenetic analyses: (i) a concatenated *rbc*L + *cox*III alignment of 101 desmid sequences selected to encompass all the main phylogenetic lineages of the family, including *Xanthidium* sequences, determined in this study; (ii) a *trn*G^{ucc} alignment of 32 newly determined *Xanthidium* sequences; and (iii) an ITS rDNA alignment comprising 27 new *Xanthidium* sequences. The list of all the sequences involved in phylogenetic analyses, including the GenBank accession numbers, is given in Table S1 in the Supporting Inforamtion. The final *rbc*L + *cox*III alignment was generated as follows: First, we downloaded 45 core *rbc*L + *cox*III sequences from the GenBank database that encompassed most of the Desmidiales lineages according to Hall et al. (2008). Then, we added 35 *rbc*L sequences selected according to the desmid phylogeny recently published by Gontcharov and Melkonian (2011) to cover the remaining Desmidiales lineages. Finally, 5 *rbc*L and 14 *cox*III sequences determined in this study together with six closely related sequences revealed by BLAST searches were added to the alignment and manually aligned in MEGA 4. The concatenated 1,870-bp matrix contained 101 taxa and was 88% filled for the *rbc*L data and 59% filled for the *cox*III data. The *trn*G^{ucc} and ITS rDNA sequences were manually aligned in MEGA 4 (Kumar et al. 2008). ITS sequences were aligned with the help of their rRNA secondary structure information, constructed using the mfold computer program, ver. 2.3 (Zuker 2003). All alignments are available in Table S1.

Table 2. List of primers used for PCR amplification and sequencing.

Primer name	Primer sequence (5′–3′)	Reference
*rbc*L		
rbcL-Pleurot-F	GGT TAA AGA TTA TAG ACT TAC	Škaloud et al. (2012)
rbcL-Pleurot-R	CCT TGA CGA GCA AGA TCA CG	Škaloud et al. (2012)
*trn*G^{ucc}		
trnG-F	AGC GGG TAT AGT TTA GTG GT	Neustupa et al. (2010)
trnG-R	GGT AGC GGG AAT CGA ACC CGC	Neustupa et al. (2010)
*cox*III		
COX-ZYG-F3	TTA CTG GAG GTG GCA CAC TT	Škaloud et al. (2011)
COX-ZYG-R2	TCC ATG AAA TCC AGT AGC TAA G	Škaloud et al. (2011)
ITS rDNA		
ITS1	TCC GTA GGT GAA CCT GCG G	White et al. (1990)
ITS4	TCC TCC GCT TAT TGA TAT GC	White et al. (1990)
ITS2N	TCG CTG CGT TCT TCA TC	Beck et al. (1998)
ITS3N	GAT GAA GAA CGC AGC GA	Beck et al. (1998)

Model selection and phylogenetic analyses. A suitable partitioning strategy and partition-specific substitution models for the *rbc*L + *cox*III data set were selected in a multi-step process (Verbruggen et al. 2010, Škaloud et al. 2012). The BIC-based model selection procedure selected the following partitioning strategy: (i) First and second codon position of *rbc*L (GTR + Γ); (ii) third codon position of *rbc*L (GTR + Γ); (iii) second codon position of *cox*III (HKY + Γ); and (iv) third codon position of *cox*III (GTR + Γ). The most appropriate substitution models for the *trn*G^{ucc} and ITS rDNA data sets were estimated using the Akaike information criterion (AIC) with PAUP/MrModeltest 1.0b (Nylander 2004). The phylogenetic trees were inferred with Bayesian inference (BI) using MrBayes, version 3.1 (Ronquist and Huelsenbeck 2003). The analysis of the *rbc*L + *cox*III data set was carried out on a partitioned data set using a covarion-like substitution model and the strategy selected during the multi-step process described above. The calculation was performed on the 86 unique sequences. The analysis of the *trn*G^{ucc} data set was performed on the 14 unique sequences by using a GTR + I substitution model. The analysis of the ITS rDNA region was carried out on a partitioned data set by using a SYM + Γ model for ITS1, a GTR + Γ model for ITS2, and a JC model for 5.8 rRNA partition. The calculation was performed on 19 unique sequences. All the parameters were unlinked among partitions. In the BI analyses, two parallel Markov chain Monte Carlo (MCMC) runs were carried out for 3 million generations,

TABLE 3. PCR cycling conditions.

Region	Initial denaturation	Denaturation	Annealing	Extension	Cycles	Final extension
*rbc*L	94°C (4 min)	94°C (1 min)	54°C (1 min)	72°C (2.0 min)	35×	72°C (10 min)
*trn*G^{ucc}	94°C (2 min)	94°C (1 min)	62°C (1 min)	72°C (1.5 min)	40×	72°C (10 min)
*cox*III	95°C (2 min)	94°C (1 min)	50°C (1 min)	72°C (1.5 min)	37×	72°C (10 min)
ITS rDNA	94°C (5 min)	94°C (1 min)	50°C (1 min)	72°C (1.5 min)	35×	72°C (10 min)

each with one cold and three heated chains. Trees and parameters were sampled for every 100 generations. Convergence of the two cold chains was checked and "burn-in" was determined using the "sump" command. Bootstrap analyses were performed by maximum likelihood (ML) and weighted parsimony (wMP) criteria using GARLI, version 0.951 (Zwickl 2009) and PAUP*, version 4.0b10 (Swofford 2002), respectively. ML analyses consisted of rapid heuristic searches (100 pseudo-replicates) using automatic termination (genthreshfortopoterm command set to 100,000). The wMP bootstrapping (1,000 replications) was performed using heuristic searches with 100 random sequence addition replicates, Tree bisection reconnection swapping, random addition of sequences (the number limited to 10,000 for each replicate), and gap characters treated as a fifth character state. The weight to the characters was assigned using the rescaled consistency index on a scale of 0–1,000. New weights were based on the mean of the fit values for each character over all of the trees in memory.

Morphometric analyses. For each strain, 20–25 adult semicells were randomly chosen for geometric morphometric investigation. In total, 10 fixed landmarks were depicted in different positions on the semicells, including the tips of the spines. In addition, 12 sliding landmarks, depicting outline curves along the semicell outlines were also digitalized (Fig. 1). For the details of the landmark digitalization on desmid semicells and description of different landmark types, see Neustupa et al. (2010) and Nemjová et al. (2011). The TPS-series software (available at http://life.bio.sunysb.edu/morph/) was used for most of the morphometric analyses. The generalized Procrustes analysis (GPA) standardized the size and optimized their rotation and translation so that the distances between the corresponding landmarks of the investigated objects were minimized (Zelditch et al. 2004). Correlation between Procrustes and the Kendall tangent space distances was assessed to ensure that the variation in shape was small enough to allow subsequent analyses (Zelditch et al. 2004). Indeed, this correlation was very high ($r = 0.999$), and hence, we proceeded with further statistical analyses. The landmark configurations of the semicells were symmetrized according to Klingenberg et al. (2002). The principal component analysis (PCA) of geometric morphometric data was conducted on the entire set of 805 semicells acquired from 33 *Xanthidium* strains. Scores of the objects on the non-zero principal component (PC) axes were used for the canonical variates analysis (CVA) aimed at separation of individual phylogenetic lineages. The significance of this analysis was assessed by the Wilk's λ in PAST, ver. 2.13 (Hammer et al. 2001). The leave-out cross-validation tests were also conducted to test for the group assignment of individual semicells on the basis of geometric morphometric data. Similarly, PCA was separately conducted on the set of seven *X. cristatum* strains and shape separation of individual semicells into three groups defined by molecular data was tested by the canonical discrimination analysis. The characteristic cell shapes of individual groups were reconstructed in TpsSuper, ver. 1.14. The Procrustes distances in shape of individual semicells were plotted against the Kimura 2-parameter genetic distances acquired from the molecular data. The genetic distances among strains evaluated by the ITS1, ITS2, ITS1 + 2, and *trnG*^{ucc} markers were used in four separate linear regression analyses. The F-tests for the equality of regression slopes between pairs of individual analyses were used to test for the differences in correlation of shape characteristics of semicells and genetic distances evaluated by different molecular markers.

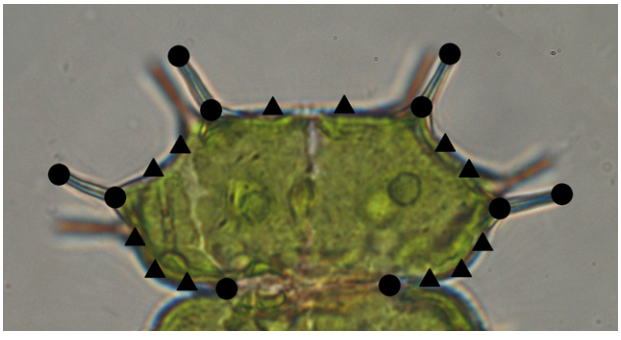

FIG. 1. Position of landmarks (circles) and semi-landmarks (triangles) on a semicell of *Xanthidium antilopaeum*.

RESULTS

Morphology of strains. The cells of all the investigated *Xanthidium* strains were readily identifiable as either *X. antilopaeum* or *X. cristatum*. Within *X. cristatum*, the cells of all strains had 10 spines per semicell, divided into four pairs and two singles (Fig. 2, A–C). However, within the traditional species boundaries, there still were remarkable differences in the morphology of individual strains (Figs. 2–5). Most of these differences corresponded to taxonomic definitions of traditional subspecific taxa, such as individual varieties. The strains representing *X. cristatum* var. *cristatum* Ralfs (H 59, ASW 07060, and ASW 07101) had relatively small cells (~40 × 35 μm without spines) and either one or two tubercles in the semicell center (Fig. 4A). In some cells, the tubercles were strongly reduced or even lacking. Conversely, cells of *X. cristatum* var. *uncinatum* Ralfs (H 12) were distinctly larger than the nominate variety (~60 × 55 μm without spines) and they differed by the upwards curved paired spines and the characteristic central ornamentation consisting of a circle of large granules (Fig. 4B). Finally, the characteristic feature of strains representing *X. cristatum* var. *scrobiculatum* Scott et Grönblad (H 08, H11, and ASW 07102) was their central ornamentation that was built of a variable number of shallow pits (scrobiculae; Fig. 4C).

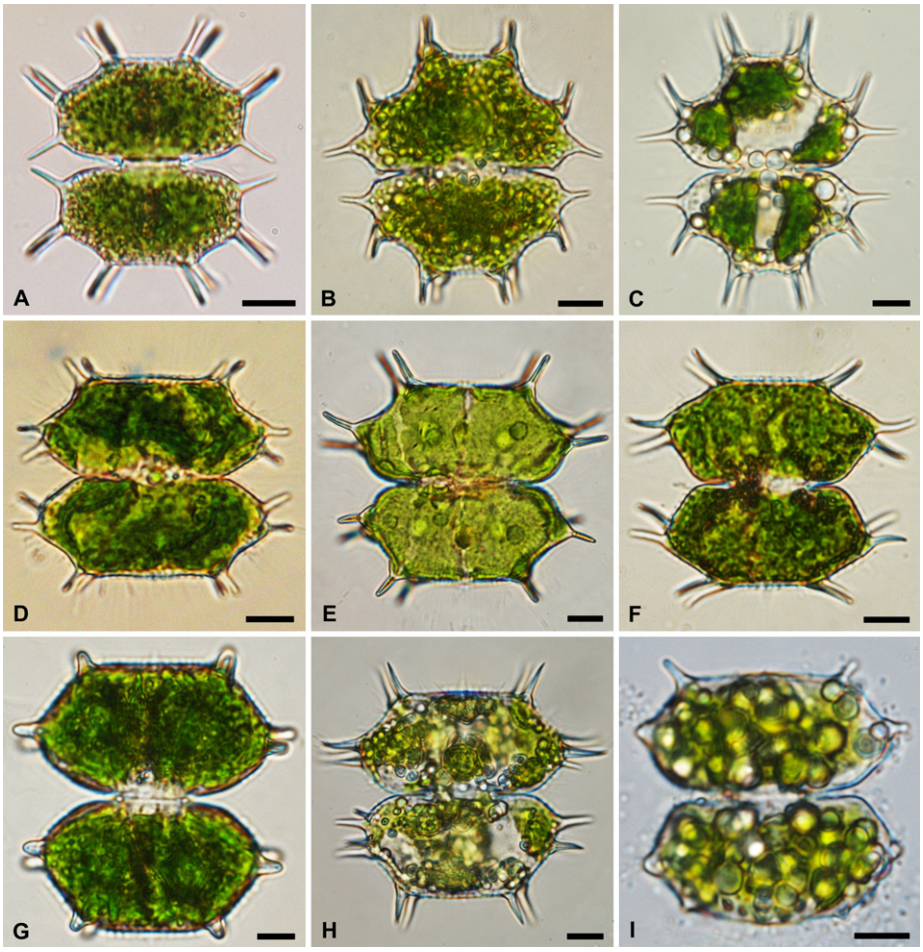

FIG. 2. LM pictures of selected strains. (A) *Xanthidium cristatum* var. *cristatum*, strain H 59. (B) *X. cristatum* var. *uncinatum*, strain H 12. (C) *X. cristatum* var. *scrobiculatum*, strain H 08. (D) *X. antilopaeum* var. *antilopaeum*, strain H 32. (E) *X. antilopaeum* var. *basiornatum*, strain H 17. (F) *X. antilopaeum* var. *planum*, strain H 18. (G) *X. antilopaeum* var. *laeve*, strain H 20. (H) *X. antilopaeum* var. *polymazum*, strain H 30. (I) *X. antilopaeum* var. *minneapoliense*, strain SVCK 147. Scale bar = 10 μm.

Within *X. antilopaeum*, all the strains had eight spines per semicell, but they were mutually different because of the arrangement of the spines, the pattern of the central scrobiculae, and the cell dimensions. Most of the strains (H 21, H 23, H 25, H 27, H 29, H 31, H 32, and SVCK 28) fitted well into the diagnosis of the nominate variety of *X. antilopaeum*. This has been characterized by comparatively wide cells and the central ornamentation consisting of an approximately elliptical group of shallow pits (Fig. 4D). The morphology of strain H 17 perfectly corresponded to that of *X. antilopaeum* var. *basiornatum* B. Eichler et Raciborski. This taxon has been distinguished on the basis of spines with a stout base, by a distinct central protuberance, and particularly by a horizontal series of 12–14 supraisthmial shallow pits located immediately above the isthmus (Fig. 4E). In *X. antilopaeum* var. *planum* Roll (H 15, H 18, H 28, and SVCK 74) both the apical and lateral spines were downwards curved and the central ornamentation was built of a central protuberance surrounded by a circle of shallow pits (Fig. 4F). The single strain identified as *X. antilopaeum* var. *laeve* Schmidle (H 20) was characterized by large and comparatively long cells (~75 × 60 μm without spines) with a relatively open sinus. The cell wall was either smooth or a central group of several shallow pits was present (Fig. 4G). *Xanthidium antilopaeum* var. *polymazum* Nordst. (H 30) was differentiated by conspicuous ornamentation consisting of a transversal, subapical arc of granules (Fig. 4H). *Xanthidium antilopaeum* var. *minneapoliense* Wolle (SVCK 147) was typical by the presence of a subapical arc of granules and two additional spines (one on either face of the cell). However, it should be noted that these spines were often reduced to conspicuous granules (Fig. 4I) or they were even lacking in some cells. Two strains of *X. antilopaeum* var. *incrassatum* (Grönblad) Förster (H 10 and H 19) differed from the nominate variety by rather large cells (~65 × 65 μm without spines) and the cell wall thickening in the central region of the semicells. Other parts of the cell wall were either smooth, or the subapical group of indistinct shallow pits was present

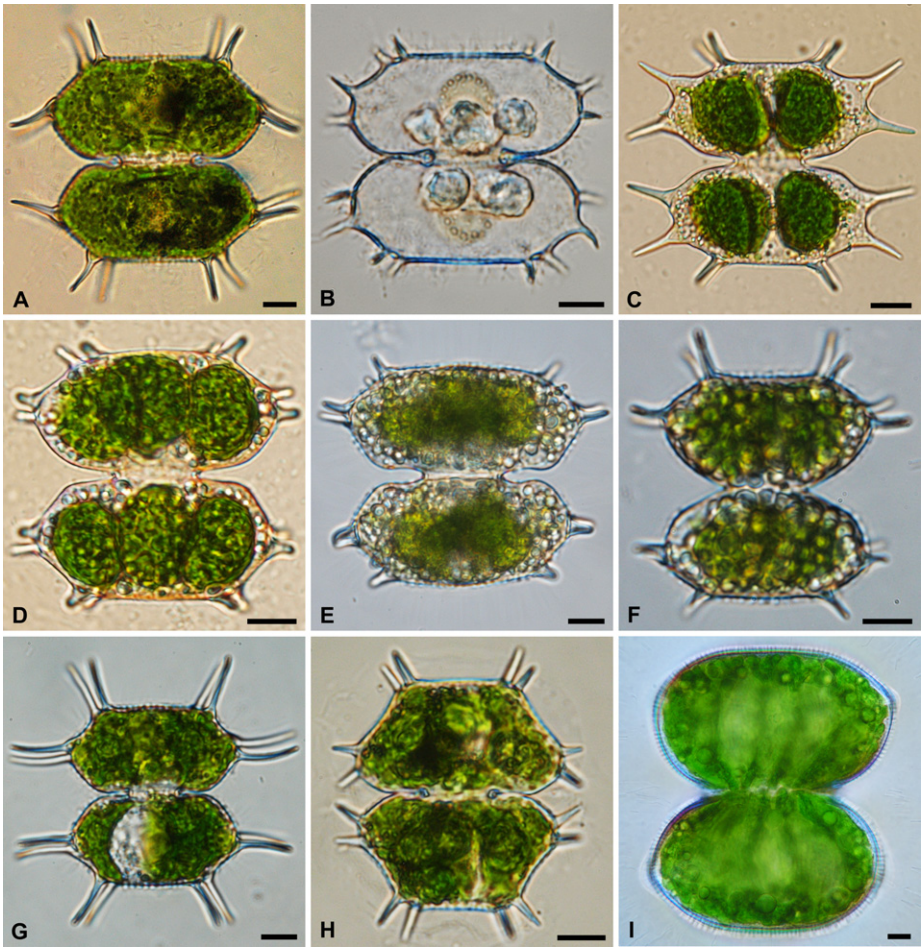

FIG. 3. LM pictures of selected strains. (A) *Xanthidium antilopaeum* var. *incrassatum*, strain H 19. (B) *X. antilopaeum* var. *depauperatum*, strain H 22. (C) *X. antilopaeum* sensu lato, strain ASW 07106. (D) *X. antilopaeum* s.l., strain ASW 07107. (E) *X. antilopaeum* s.l., strain SVCK 105. (F) *X. antilopaeum* s.l., strain SVCK 281. (G) *X. antilopaeum* s.l., strain SVCK 343. (H) *X. antilopaeum* s.l., strain H 26. (I) *Staurastrum tumidum*, strain H 76. Scale bar = 10 μm.

(Fig. 5A). Finally, *X. antilopaeum* var. *depauperatum* W. et G.S.West (strain H22) was characterized by the central ornamentation composed of two concentric rings of distinct pits surrounding a middle granula (Fig. 5B), and by obtuse lateral angles of the semicells. Conversely, another typical feature of this variety, a conspicuous variation in the number, length, and arrangement of spines (West and West 1912) was not observed. The other investigated strains (ASW 07105, ASW 07106, ASW 07107, SVCK 105, SVCK 281, SVCK 343, and H 26) fitted well into morphological species definition of *X. antilopaeum*, but they could not be determined to belong to any of the traditional varieties (Figs. 3 and 5). Morphology of our *S. tumidum* isolate (strain H 76) corresponded with the morphological delimitation of this species (Fig. 3I). LM and SEM pictures of all the strains are available online as supplementary material.

Molecular phylogenetic analyses. The Bayesian phylogenetic tree constructed on the basis of the partitioned *rbcL* + *cox*III data set (Fig. 6) inferred all the investigated *Xanthidium* strains in a single, well-resolved clade (BI/ML/MP support 1.00/98/98). Among the traditionally recognized *Xanthidium* species (*X. antilopaeum*, *X. cristatum*, *X. hastiferum*, *X. subhastiferum*, and *X. brebissonii*), this clade also comprised *S. tumidum*, a species having smooth cells lacking a series of spines that was considered typical for the genus *Xanthidium*. The *rbc*L sequences of our isolate H 76 and the strain SVCK 85 (accession no. AJ553972.1) were identical, corroborating the correct placement of *S. tumidum* within the *Xanthidium* clade. All but one of the *X. antilopaeum* strains were closely related, inferred in a single clade together with *X. cristatum*, *X. hastiferum*, and *X. subhastiferum*. The exception was *X. antilopaeum* var. *basiornatum* that formed a well-resolved clade together with *S. tumidum*. *Xanthidium armatum*, a conspicuous desmid species characteristic by stout, bi- or trifurcate spines, was recognized in a sister position to all the *Xanthidium* taxa. The relation of *X. armatum* to other *Xanthidium* taxa was moderately supported (BI/ML/MP support 0.98/-/77). Our

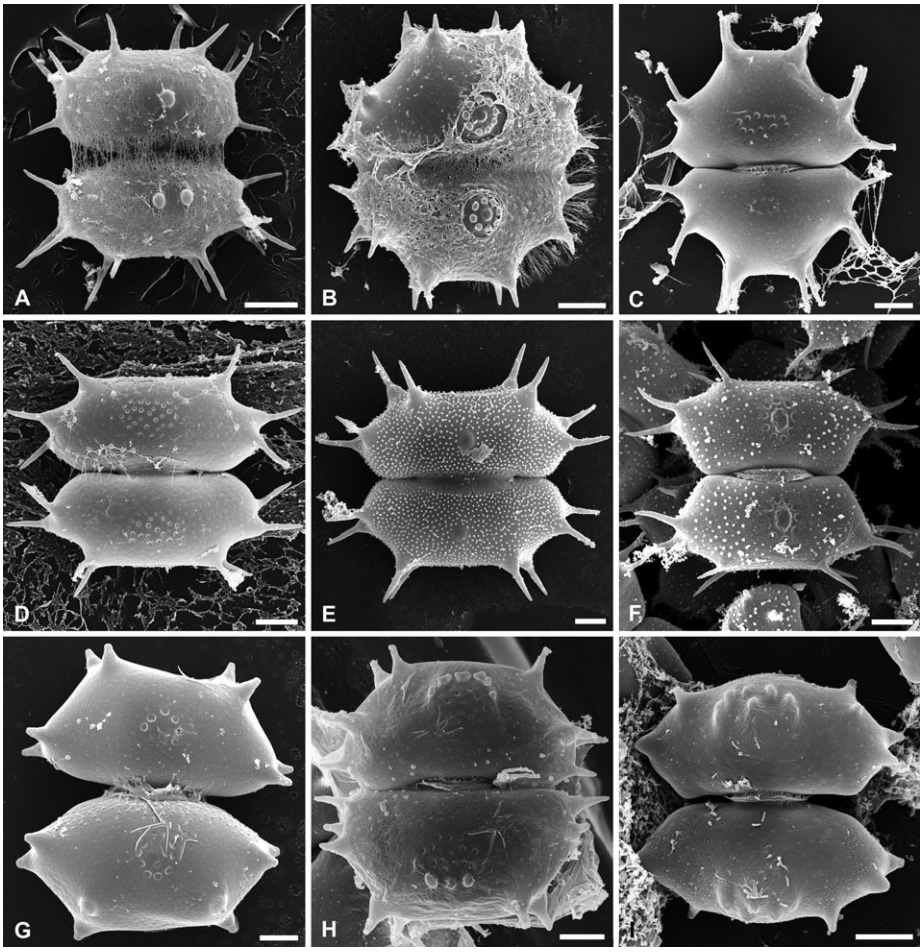

FIG. 4. SEM pictures of selected strains. (A) *Xanthidium cristatum* var. *cristatum*, strain H 59. (B) *X. cristatum* var. *uncinatum*, strain H 12. (C) *X. cristatum* var. *scrobiculatum*, strain H 11. (D) *X. antilopaeum* var. *antilopaeum*, strain H 29. (E) *X. antilopaeum* var. *basiornatum*, strain H 17. (F) *X. antilopaeum* var. *planum*, strain H 28. (G) *X. antilopaeum* var. *laeve*, strain H 20. (H) *X. antilopaeum* var. *polymazum*, strain H 30. (I) *X. antilopaeum* var. *minneapoliense*, strain SVCK 147. Scale bar = 10 μm.

phylogenetic analysis thus recognized the monophyly of almost all the *Xanthidium* species with known molecular data. The single exception was *X. octocorne*, a small desmid with cells characteristically possessing eight long spines. This species was nested within the firmly supported "*Staurodesmus* 1" lineage (*sensu* Gontcharov 2008), distantly related to the *Xanthidium* clade.

To better resolve the phylogenetic relationships of the *X. antilopaeum* and *X. cristatum* strains, we conducted further analyses of two fast-evolving loci, i.e., plastid *trn*G^{ucc} and nuclear ITS rDNA (Fig. 7). The sequencing of *trn*G^{ucc} was successful in all the 32 investigated strains; however, high-quality ITS rDNA sequences were obtained for only 27 of them. Despite repeated DNA isolation and PCR amplification, poor sequencing products were constantly obtained for the strains H18, H22, H27, H28, and SVCK 343, so that these were omitted from the ITS rDNA phylogenetic analysis. A comparison of the phylogenetic trees, estimated separately for the *trn*G^{ucc} and ITS rDNA data sets, resulted in the detection of several reciprocal monophyletic clades that were concordant between the unlinked loci. However, an obvious incongruence was detected in the topology of the uppermost clades in Figure 7 (see below). In general, both single-loci trees were congruent in resolving two major lineages corresponding to *X. antilopaeum* and *X. cristatum*. Within the latter lineage, three well-resolved clades were determined, corresponding to the traditional subspecific taxa *X. cristatum* var. *cristatum*, *X. cristatum* var. *scrobiculatum*, and *X. cristatum* var. *uncinatum*. Within the *X. antilopaeum* complex, four clades were reciprocal monophyletic: (i) the traditional subspecific taxon *X. antilopaeum* var. *planum*, (ii) a clade comprising *X. antilopaeum* var. *incrassatum* and two morphologically distinct strains SVCK 105 and SVCK 343, (iii) a clade containing morphologically about similar taxa *X. antilopaeum* var. *polymazum* and *X. antilopaeum* var. *minneapoliense*, and (iv) a poorly resolved clade of *X. antilopaeum* var. *laeve* and *X. antilopaeum*, strain H26. Three remaining *X. antilopaeum* clades inferred from the *trn*G^{ucc} data

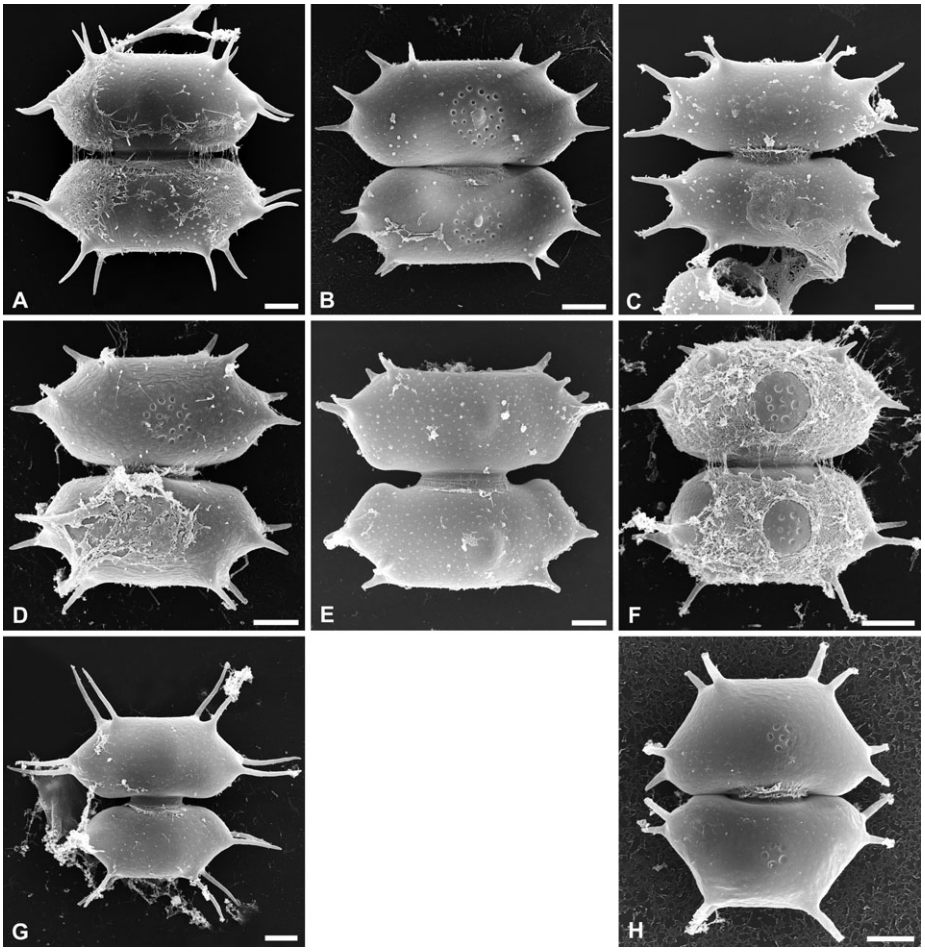

FIG. 5. SEM pictures of selected strains. (A) *Xanthidium antilopaeum* var. *incrassatum*, strain H 19. (B) *X. antilopaeum* var. *depauperatum*, strain H 22. (C) *X. antilopaeum* sensu lato, strain ASW 07106. (D) *X. antilopaeum* s.l., strain ASW 07107. (E) *X. antilopaeum* s.l., strain SVCK 105. (F) *X. antilopaeum* s.l., strain SVCK 281. (G) *X. antilopaeum* s.l., strain SVCK 343. (H) *X. antilopaeum* s.l., strain H 26. Scale bar = 10 μm.

were either polyphyletic or unresolved in the ITS rDNA phylogram. *Xanthidium antilopaeum* var. *antilopaeum* strains were resolved monophyletic in the ITS rDNA phylogenetic tree, but formed two distinct clades in the *trn*G^{ucc} phylogeny. Similarly, three *X. antilopaeum* strains ASW07105, ASW07106, and ASW07107 had identical *trn*G^{ucc} sequences, but were recovered in two different clades in the ITS rDNA tree.

Morphometric analyses. The CVA of geometric morphometric data of the entire set of 805 semicells (Fig. 8A) was analyzed to evaluate separation of *X. antilopaeum, X. cristatum* and *X. antilopaeum* var. *basiornatum* that formed three different phylogenetic lineages. The ordination resulted in their highly significant separation (Wilk's $\lambda = 0.094$, $P < 0.0001$). The leave-one-out cross-validation tests illustrated that the canonical discriminant function correctly classified 97.9% of the *X. antilopaeum* semicells. In addition, there was 99.4% correct classification of *X. cristatum*, and 100% correct classification of *X. antilopaeum* var. *basiornatum* semicells. The separate analysis of 163 semicells focused on the *X. cristatum* cluster (Fig. 8B) revealed strong shape separation of three phylogenetic lineages within this traditional morphospecies (Wilk's $\lambda = 0.015$, $P < 0.0001$). The cross-validation tests illustrated the 100% correct classification of the *X. cristatum* var. *uncinatum* and *X. cristatum* var. *cristatum* semicells; whereas there were 98.7% of the *X. cristatum* var. *scrobiculatum* semicells correctly classified on the basis of geometric morphometric data.

The linear regression analyses of morphometric versus genetic distances illustrated that the distance in shape of semicells was significantly related to their genetic distances (Fig. 9). However, this relation was relatively weak in the ITS1, ITS2, and ITS1 + two regions. Conversely, a stronger relation was revealed between the Procrustes distance and the Kimura 2-parameter distance evaluated by the sequences of the *trn*G^{ucc} plastid encoded marker. This difference in relation of morphology and sequence data evaluated by different molecular markers was also confirmed by the F-tests for the equality of regression

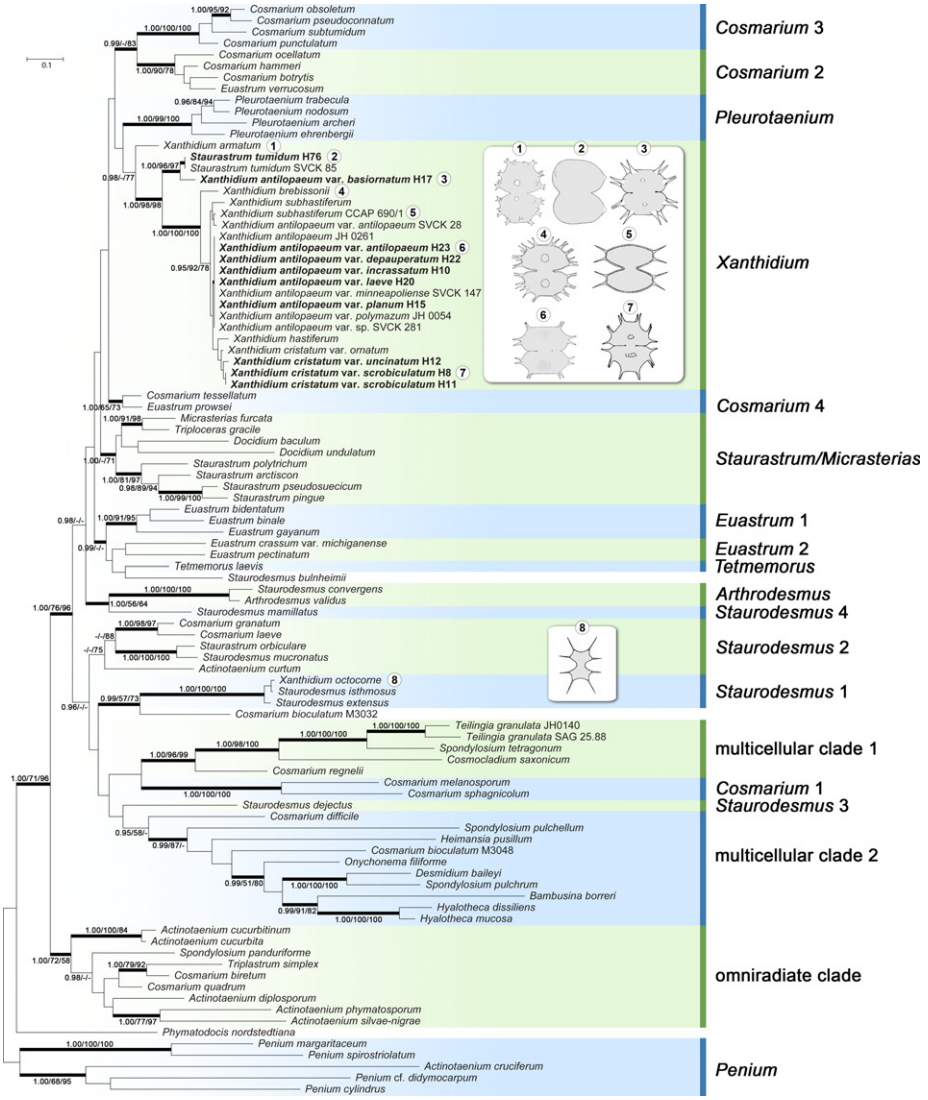

FIG. 6. Bayesian analysis based on the combined and partitioned *rbc*L + *cox*III data set of Desmidiaceae. Four partitions were analyzed separately by using a GTR + Γ model for the first and second codon positions of the *rbc*L gene, GTR + Γ model for the third codon position of the *rbc*L gene, HKY + Γ model for the first and second codon positions of the *cox*III gene, and GTR + Γ model for the third codon position of the *cox*III gene, under the covarion model. Values at the nodes indicate statistical support estimated by three methods —MrBayes posterior-node probability (left), maximum-likelihood bootstrap (in the middle), and maximum-parsimony bootstrap (right). Thick branches represent nodes receiving the high PP support (≥ 0.99). Species affiliation to 19 desmid clades *sensu* Gontcharov and Melkonian (2011) is indicated. Morphology of the selected investigated strains is given in the boxes and linked to corresponding sequences by numbers. Scale bar shows the estimated number of substitutions per site.

slopes among individual analyses. The slope of *trn*G^{ucc}-based regression analysis differed significantly from slopes of all the three remaining analyses (F = 11.65–13.48, $P = 0.0003$–0.0007). On the other hand, the differences among slopes of regression analyses based on different parts of the ITS region were insignificant (F = 0.08–0.99, $P > 0.05$).

DISCUSSION

Our molecular phylogenetic analyses based on the partitioned *rbcL* + *cox*III data set confirmed the monophyly of almost all the traditional *Xanthidium* species examined, including our target taxa *X. antilopaeum* and *X. cristatum*. This has previously been indicated by other authors as well (Hall et al. 2008, Gontcharov and Melkonian 2011). The single exception was *X. octocorne*, which was nested within the firmly supported "*Staurodesmus* 1" clade (*sensu* Gontcharov 2008). Since this strongly supported lineage also contains *Staurodesmus triangularis* (Lagerheim) Teiling (Gontcharov and Melkonian 2011), the type species of the genus *Staurodesmus* (Compère 1977), we decided to establish a new combination *Staurodesmus octocornis* (see chapter Taxonomical consequences). This separation of *X. octocorne* from *Xanthidium* is a logical consequence of its longtime recognized controversial taxonomical position.

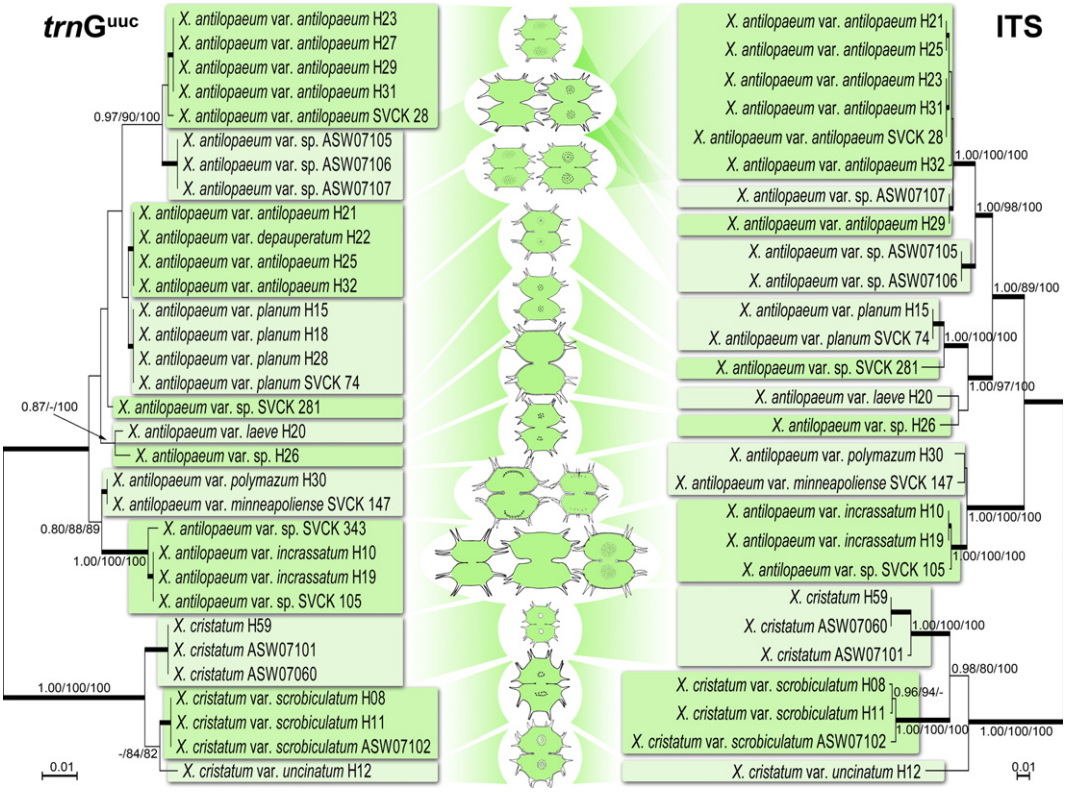

FIG. 7. Phylogenetic trees of *Xanthidium cristatum* and *X. antilopaeum* taxa derived from Bayesian analyses of chloroplast *trn*G^{ucc} and nuclear ITS rDNA sequences, using a GTR + I model for the *trn*G^{ucc} *rbc*L gene, GTR + Γ model for the ITS1 region, GTR + I model for the ITS2 region, and the JC model for the 5.8 rDNA region. Values at the nodes indicate statistical support estimated by three methods—MrBayes posterior-node probability (left), maximum-likelihood bootstrap (in the middle), and maximum-parsimony bootstrap (right). Thick branches represent nodes receiving the highest PP support (1.00). A scale bar shows the estimated number of substitutions per site. See text for details of discordance between the two topologies.

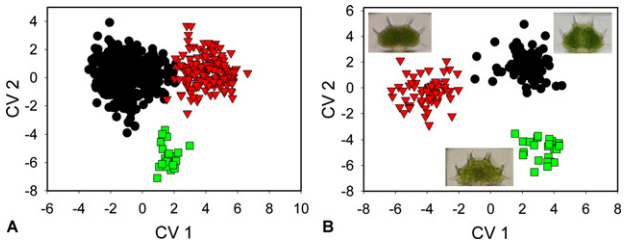

FIG. 8. Multivariate analyses of geometric morphometric data. (A) The ordination plot of first and second axes of the canonical variates analysis (CVA) of all the 805 investigated objects aimed at morphological separation of three phylogenetic lineages. Circles, *X. antilopaeum* sensu lato; triangles, *X. cristatum* sensu lato, squares, *X. basiornatum*. (B) The ordination plot of first and second axes of the canonical variates analysis (CVA) separating three phylogenetic species of the traditional *X. cristatum* lineage. Triangles, *X. cristatum* var. *cristatum*; circles, *X. cristatum* var. *scrobiculatum*; squares, *X. cristatum* var. *uncinatum*.

Xanthidium octocorne does not match the morphological characteristics of the genus, having no central protuberance and only a single series of spines. It is likely that some other *Xanthidium* species with a similar morphology, such as *X. smithii*, *X. impar*, or *X. bifidum*, may in fact also be a part of the *Staurodesmus* lineage. However, this hypothesis requires further molecular phylogenetic confirmation.

The analysis of the *rbcL* + *cox*III data set also confirmed the unexpected phylogenetic position of *S. tumidum*, which was already suggested by Gontcharov et al. (2003). The phylogenetic analysis of two different *S. tumidum* strains significantly inferred both isolates into the above-mentioned robust *Xanthidium* clade. Having three- or four-radiate, smooth cells lacking a series of spines typical for the genus, this large and conspicuous desmid matches the generic diagnosis of *Xanthidium* even less than *X. octocorne* (e.g., Coesel and Meesters 2007). However, a possible evolutionary relationship between *S. tumidum* and *X. armatum* has already been suggested by Meindl (1986) and Höftberger and Meindl (1993) on the basis of their similar, peculiar way of nuclear migration during the semicell morphogenesis. Such a morphological peculiarity within a well-supported monophyletic genus may be no exception among Desmidiales. Recently, Škaloud et al. (2011) illustrated that three species, originally belonging to the morphologically distinct genera *Cosmarium*, *Triploceras*, and *Staurodesmus* actually belong to the genus

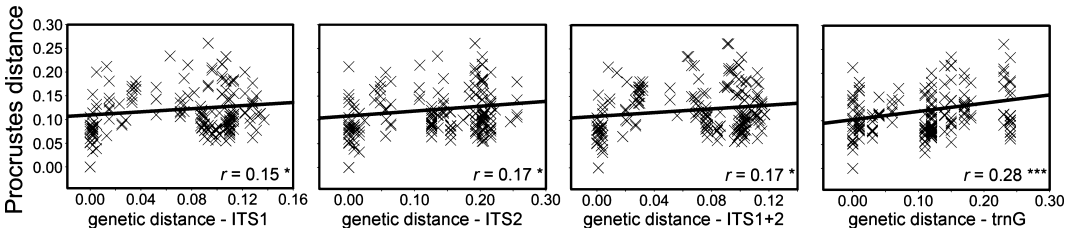

FIG. 9. Linear correlation analyses of morphometric differences among strains (Procrustes distance) and their genetic distances evaluated by the ITS1, ITS2, ITS1 + 2 and trnG^{UCC} regions. The linear correlations are represented by Pearson's *r* values. Significances are given by the *P*-values: *** $P < 0.001$, * *P*-value 0.01–0.05.

Micrasterias. The last species *M. dickiei* (Ralfs) Škaloud et al. is morphologically relatively similar to *S. tumidum*, also having three-radiate, smooth-walled cells (Coesel and Meesters 2007). Škaloud et al. (2011) illustrated hypothetic evolutionary transformation of a *M. pinnatifida*-like ancestor into *M. dickiei*. This supposedly proceeded from the occasional 3-radiate form of *M. pinnatifida* by shape simplification that usually accompanies formation of 3-radiate forms (e.g., Teiling 1956). A similar evolutionary scenario might have taken place in *S. tumidum*. Triradiate morphs of *Xanthidium* taxa have occasionally been reported (West and West 1912) and several of them were even described as separate taxa (e.g., Lundell 1871, Irénée-Marie 1939, Williamson 2002). The accompanying shape simplification would explain the loss of spines during the morphological evolution of *S. tumidum* from a *Xanthidium*-like ancestor. Similar to *X. octocorne*, the taxonomic position of *S. tumidum* has been the subject of some controversy in the past. Besides the genus *Staurastrum*, it was attributed to the genus *Staurodesmus* (e.g., Lenzenweger 1997). In addition, Wille (1890) included it in his newly created genus *Pleurenterium*. This taxon was originally described by Lundell (1871) as a subgenus of *Staurastrum*, on the basis of a different, parietal form of chloroplasts. Gay (1884) proposed to classify *Pleurenterium* as a section of *Xanthidium* on the basis of similar, parietal chloroplasts of both taxa. He also pointed out to the occasional occurrence of three-radiate forms in other species of the genus *Xanthidium*. Interestingly, presented phylogenetic data fully supported these early taxonomic studies. It is a matter of speculation whether some other morphologically similar *Staurastrum* taxa, that have been separated from *Staurastrum* into *Pleurenterium* on the basis of their parietal chloroplasts, such as *S. longispinum* (Lagerheim 1888) and *S. grande* (Wille 1890), may also belong to *Xanthidium*.

The analyses of plastid *trn*G^{ucc} and nuclear ITS rDNA resulted in trees resolving two major lineages corresponding to the traditional taxa *X. antilopaeum* and *X. cristatum* (Fig. 7). This suggests that the traditional morphology-based discriminative criteria of both species (the different number of spines per semicell) may generally still be considered relevant. However, our phylogenetic analyses also suggested that *X. antilopaeum* var. *basiornatum* does not belong to the *X. antilopaeum*/*X. cristatum* clade and forms a well-resolved independent clade together with *S. tumidum*. This would imply that *X. antilopaeum* var. *basiornatum*, although possessing eight spines per semicell like other *X. antilopaeum* taxa, in fact represents an additional separate species of the genus *Xanthidium*. This hypothesis was also corroborated by subsequent geometric morphometric analysis that unequivocally separated populations of *X. antilopaeum*, *X. cristatum*, and *X. antilopaeum* var. *basiornatum* (Fig. 8A). Therefore, we propose that the last taxon should be established as a separate species (see Taxonomical consequences). It should be noted that Förster (1983) classified *X. antilopaeum* var. *basiornatum* as a separate variety of *X. canadense* (Joshua) Förster. However, since there is a clear morphological difference between both taxa, Förster's opinion has not been generally accepted, and *X. antilopaeum* var. *basiornatum* has in reputable desmid monographs (e.g., Lenzenweger 1997) still been kept as a variety of *X. antilopaeum*. We can see that the taxonomic dilemma concerning the correct classification of this taxon has also been reflected by its isolated phylogenetic position. However, the molecular data, together with the morphometric analysis, unequivocally indicated that *X. basiornatum* should be treated as a separate species.

The molecular data revealed three well-resolved clades within traditional *X. cristatum* that corresponded to the traditional varieties *X. cristatum* var. *cristatum*, *X. cristatum* var. *scrobiculatum*, and *X. cristatum* var. *uncinatum*. This classification pattern was also confirmed by the geometric morphometric analysis that illustrated highly significant semicell shape differences among these three taxa (Fig. 8B). These results, together with the fact that the general morphology of *X. cristatum* var. *uncinatum* and *X. cristatum* var. *scrobiculatum* is clearly different from the nominate variety (compare Figs. 2, A–C and 4, A–C, see also Appendix S1 in the Supporting Information), led us to the conclusion that they should be regarded as separate species (see Taxonomical consequences). Conversely, *X. cristatum* var. *bituberculatum*, described by Lowe (1923), which differs from the nominate variety basically by the presence of two tubercles instead of one in the central area of the semicells, should not be considered a separate taxon. As already mentioned above, the form of central

ornamentation in *X. cristatum* may be extremely variable. The single strain ASW 07060 had either one tubercle or the central ornamentation was completely lacking. Semicells with either one or two tubercles were also found in strains ASW 07101 and H 59. The latter strain even had numerous Janus cells with the semicells corresponding either to *X. cristatum* var. *bituberculatum* or to *X. cristatum* var. *cristatum* (Fig. 4A, see also Appendix S1). Therefore, traditional *X. cristatum* var. *bituberculatum* should be considered an ecomorph of *X. cristatum* sensu stricto.

Comparing the lineages that were delineated within the traditional *X. antilopaeum* complex using the chloroplast and nuclear sequences, we observed a large degree of congruence. Nearly all the *trn*G^{ucc} clusters were resolved as monophyletic lineages in the ITS rDNA data set (Fig. 7). However, incongruence among loci was detected in the topology of strains H 21, H 22, H 23, H 25, H 27, H 29, H 31, H 32, SVCK 28, ASW 07105, ASW 07106, and ASW 07107. The most likely explanation of this phenomenon is that the branching order of the "species tree" might differ from that of the "genes tree" because of incomplete lineage sorting from an ancestral polymorphic gene pool (Pamilo and Nei 1988, Rosenberg 2003). Accordingly, the conflicting topologies could be caused by different rates of loci coalescence and the stochastic processes of loci differentiation (Carstens and Knowles 2007). The observed mismatch among gene trees indicated rather rapid diversification within the *X. antilopaeum* complex that could not be unambiguously differentiated by analyzing the single loci. Conversely, analyses of multiple loci and multiple sequences per loci could give a more complete picture of phylogenetic divergence among closely related species within the *X. antilopaeum* complex. Unfortunately, since the life histories inferred by the *trn*G^{ucc} and the ITS rDNA data sets are not congruent, we cannot resolve the real "species tree" without analyzing additional rapidly evolving genetic loci. Nevertheless, we have several indications that favored the *trn*G^{ucc} evolutionary scenario over the ITS rDNA topology. First, the clades inferred by the *trn*G^{ucc} phylogeny showed an apparent biogeographic pattern, suggesting the distributional differences of the recently diverged species (see next). Second, reliability of the plastid *trn*G^{ucc} data has been supported by the population genetic theory, which predicts that inferences from nuclear DNA are often confounded by their four times longer coalescent time in comparison with organelle DNA (Moore 1995). Consequently, the failure to obtain high-quality ITS rDNA sequences for all the *X. antilopaeum* strains could be explained by the existence of many paralogous copies of the ITS rDNA locus, which have not yet been sufficiently homogenized by concerted evolutionary processes (Rich et al. 1997). Finally, reliability of the *trn*G^{ucc} data set to resolve the real "species tree" has also been supported by the significantly better linear correlation between the matrices of morphological differences and the *trn*G^{ucc}-based genetic distances among *X. antilopaeum* strains, as compared with the ITS rDNA data set (Fig. 9). These results indicated the limited gene flow among the lineages as delineated by *trn*G^{ucc}-based phylogeny, resulting in subtle morphological differences among the recently diversified species. Summing up, the *trn*G^{ucc} sequences could provide good molecular markers for the species delimitation in *X. antilopaeum* species complex, even though they were less variable than the ITS rDNA sequences. The usefulness of the *trn*G^{ucc} intron sequences for resolving intraspecific diversity within various desmid species complexes has recently been also shown by Neustupa et al. (2010, 2011b), Nemjová et al. (2011), and Škaloud et al. (2012). We therefore believe that the *trn*G^{ucc} marker should be considered a good candidate for a green algal barcode, in particular for Streptophytes (Shaw et al. 2005, Hall et al. 2010). Furthermore, the phylogenetic tree inferred from the *trn*G^{ucc} sequences could provide insights into the morphological evolution within the *X. antilopaeum* species complex. For example, the rapid morphological diversification has been observed in a morphologically very diverse group of *X. antilopaeum* var. *incrassatum* and strains SVCK 105 and SVCK 343. On the other hand, genetically identical taxa *X. antilopaeum* var. *polymazum* and *X. antilopaeum* var. *minneapoliense* shared a great deal of morphological similarity (Fig. 4, H–I). Already Grönblad (1921) pointed out to the fact that the accessory subapical spines in *X. antilopaeum* var. *minneapoliense*, which are the only distinguishing characteristic between both these varieties, may very often be reduced, or even absent, and that these two varieties would better be merged together. As our morphological observations fully confirmed the Grönblad's (1921) data, we can conclude that *X. antilopaeum* var. *minneapoliense* may most probably only represent the ecomorph of *X. antilopaeum* var. *polymazum*. Despite this, we feel it is premature to propose any formal taxonomic changes within the *X. antilopaeum* complex (other than var. *basiornatum*) unless the *trn*G^{ucc} phylogeny is supported by additional molecular markers.

Recent polyphasic studies, employing light microscopic, ultrastructural, morphometric and molecular phylogenetic methods, that evaluated the validity of desmidiacean species concepts, particularly in the genus *Micrasterias* (Neustupa et al. 2010, 2011a,b, Nemjová et al. 2011), illustrated apparent pseudocryptic diversity in a number of traditional species. Several morphologically defined infraspecific taxa were shown to be artificial, but, on the other hand, several traditional varieties obviously represented independent species. Our data revealed a pattern similar to the above-mentioned studies. Although several examples of ill-defined traditional subspecific taxa were found (*X. cristatum* var. *bituberculatum* and *X. an-*

tilopaeum var. *minneapoliense*), the major part of morphological variability among the investigated strains was phylogenetically relevant. Consequently, several infraspecific taxa should now be established as separate species. This is fully in accordance with the view of Kouwets (2008) who stated, "In desmids, to achieve a feasible taxonomy, 'stable' varieties should generally be given the status of a separate species. The taxonomic status of 'forma' should be abandoned altogether. Morphological variations induced by the environment should merely be characterized as 'ecomorpha' without any taxonomic status." It is obvious, however, that in this respect, phylogenetic species-level desmid taxonomy is still at the beginning.

Brook (1981) estimated that more than 6,000 species of desmids have been described from all parts of the world. However, the recent studies on phylogenetic species concepts in desmid taxa (Neustupa et al. 2010, 2011a,b, Nemjová et al. 2011, Škaloud et al. 2012, this study) unanimously illustrated that some traditional morphological species (such as *M. truncata*, *M. fimbriata*, *Pleurotaenium ehrenbergii*, or *X. cristatum*) actually consist of at least two or three phylogenetic species recognizable using morphometric methods. Conversely, the number of traditional taxa that were found phylogenetically homogenous (such as *M. rotata* or *Pleurotaenium archeri*) was distinctly lower. Therefore, we believe that with the wide employment of the molecular methods in species-level taxonomy of Desmidiales, about twice-as-many species may be recognized than previously described on the basis of purely morphological data.

The above-mentioned studies on species concepts of desmids also revealed a clear geographic signal among several investigated species indicating that the actual species diversity of these relatively large protists may be related to either the patterns of their geographic distribution or the macroscale climatic factors. The phylogenetic structure of the *M. cruxmelitensis/M. radians* complex (Neustupa et al. 2010) reflected the origin of strains, separating the European, African, and Asian strains. Nemjová et al. (2011) concluded that the Australian strains of the traditional *M. truncata* probably represented a separate species. Neustupa et al. (2011b) illustrated that the two firmly delimited phylogenetical lineages within the conspicuous desmid species *M. fimbriata* exhibited largely disparate geographic distribution patterns across Europe. Although we only analyzed European and North American isolates, our results certainly do not contradict the above-mentioned observations. The phylogenetic tree based on the *trn*G^{ucc} data set indicated several examples of possible geographical restriction among *Xanthidium* phylogenetic taxa. All the three strains of traditional *X. antilopaeum* (ASW 07105, ASW 07106, and ASW 07107) that originated from arctic regions (Greenland, St. Matthew Island in the Bering Sea, respectively) were inferred in a single clade (Fig. 7). In addition, the phylogenetic analysis also separated the central European and western European representatives of *X. antilopaeum* var. *antilopaeum* (Fig. 7), indicating a geographic pattern very similar to that observed in two phylogenetic species of traditional *M. fimbriata* (Neustupa et al. 2011a,b). The differences in distribution pattern may also be anticipated in three phylogenetic taxa of *X. cristatum*. Whereas the nominate variety and var. *uncinatum* are relatively common all across Europe (West and West 1912, Lenzenweger 1997, Kouwets 1999, Abdelahad et al. 2003, Coesel and Meesters 2007, Šťastný 2010), we could not find any reliable report of morphotypes corresponding to var. *scrobiculatum* outside the western European regions typical with the oceanic climate.

Taxonomic consequences. On the basis of the data presented in this study, some taxonomical changes appeared to be necessary. By the transfer of *X. octocorne* to *Staurodesmus*, the genus *Xanthidium* formally remains monophyletic. Since a type species of *Xanthidium* has not yet been designated (Ralfs 1848, Guiry and Guiry 2012), and the definition of a type species is crucial for the nomenclatural identity of a genus, we state, in accordance with the ICBN article 37.3 (McNeill et al. 2006), that *X. cristatum*, one of the species that have originally been included into the genus *Xanthidium* by Ralfs (1848), should be the type species of this genus.

Xanthidium Ralfs 1848, Brit. Desmidieae, p. 111.

Type species (here designated): *Xanthidium cristatum* Ralfs 1848, Brit. Desmidieae, p. 115, Pl. 19, Fig. 3A–C.

Synonym: *Xanthidium cristatum* var. *bituberculatum* Lowe 1923, Canadian Arctic Exped. 4: p. 27, Fig. 4.

Staurodesmus octocornis (Ralfs) Stastny, Skaloud et Neustupa **comb. nov.**

Basionym: *Xanthidium octocorne* Ralfs 1848, Brit. Desmid., p. 116, Pl. 20, Fig. 2.

Synonym: *Arthrodesmus octocornis* (Ralfs) Archer in Pritchard 1861, Hist. Inf., p. 736.

Xanthidium tumidum (Ralfs) Stastny, Skaloud et Neustupa **comb. nov.**

Basionym: *Staurastrum tumidum* Ralfs 1848, Brit. Desmid., p. 126, Pl. 21, Fig. 6.

Synonyms: *Staurodesmus tumidus* (Ralfs) Teiling, 1967, Ark. F. Bot., II, 6(11), p. 578, Pl. 22, Fig. 1; *Pleurenterium tumidum* (Bréb.) Wille 1890, Engler & Prantl, Nat. Pflanzenfam. 1890, p. 11.

Xanthidium basiornatum (B.Eichler et Raciborski) Stastny, Skaloud et Neustupa **comb. nov. et stat. nov.**

Basionym: *Xanthidium antilopaeum* var. *basiornatum* B.Eichler et Raciborski 1893, Rozpr. Akad. Umiej. Wydz. Mat.-Przyr. Krakowie, II, 26, p.125, Pl. 3, Fig. 31.

Synonym: *Xanthidium canadense* (Joshua) Förster var. *basiornatum* (B.Eichler et Raciborski) Förster 1983, Algol. Studies 33, p. 378, Fig. 4.

Xanthidium uncinatum (Ralfs) Stastny, Skaloud et Neustupa **comb. nov. et stat. nov.**

Basionym: *Xanthidium cristatum* var. *uncinatum* Ralfs 1848, Brit. Desmid., p. 115, Pl. 19, Fig. 3D–F.

Xanthidium scrobiculatum (Scott et Grönblad) Stastny, Skaloud et Neustupa **comb. nov. et stat. nov.**

Basionym: *Xanthidium cristatum* var. *scrobiculatum* Scott et Grönblad 1957, Acta Soc. Sci. Fennicae, II, B, 2(8), p. 30, Pl. 17, Figs 3–6.

We are indebted to Petra Wagner and Barbara Melkonian for their kind provision of strains from the SVCK and ASW culture collections. The Editage company is acknowledged for the revision of the English language. The study was supported by Grant no. 206/09/0906 of the Czech Science Foundation.

Abdelahad, N., Bazzichelli, G. & D'Archino, R. 2003. *Catalogo delle Desmidiaceae (Chlorophyta, Zygnematophyceae) segnalate in Italia. [A checklist of Desmids (Chlorophyta, Zygnematophyceae) reported in Italy].* Academia Nazionale delle Science detta dei XL, Roma, 102 pp.

Beck, A., Friedl, T. & Rambold, G. 1998. Selectivity of photobiont choice in a defined lichen community: inferences from cultural and molecular studies. *New Phytol.* 139:709–20.

Beszteri, B., Ács, E. & Medlin, L. 2005. Conventional and geometric morphometric studies of valve ultrastructural variation in two closely related *Cyclotella* species (*Bacillariophyta*). *Eur. J. Phycol.* 40:89–103.

Blackburn, S. I. & Tyler, P. A. 1987. On the nature of eclectic species – a tiered approach to genetic compatibility in the desmid *Micrasterias thomasiana. Br. Phycol. J.* 22:277–98.

Brook, A. J. 1981. *The Biology of Desmids.* University of California Press, Berkeley, California, 276 pp.

Carstens, B. C. & Knowles, L. 2007. Estimating species phylogeny from gene-tree probabilities despite incomplete lineage sorting: an example from *Melanoplus* grasshoppers. *Syst. Biol.* 56:400–11.

Coesel, P. F. M. 1984. Taxonomic implications of SEM revealed cell wall sculpturing in some small-sized desmid species (Chlorophyta, Conjugatophyceae). *Acta Bot. Neerl.* 33:385–98.

Coesel, P. F. M. 2001. A method for quantifying conservation value in lentic freshwater habitats using desmids as indicator organisms. *Biodiv. Conserv.* 10:177–87.

Coesel, P. F. M. 2003. Desmid floor data as a tool in conservation management of Dutch freshwater wetlands. *Biologia* 58: 717–22.

Coesel, P. F. M. 2005. Desmids in the Netherlands. Desmid of the month, October 2005. *Xanthidium antilopaeum.* Available at http://www.desmids.nl/maand/english/0510_octeng.html.

Coesel, P. F. M. & Meesters, J. 2007. *Desmids of the Lowlands. Mesotaeniaceae and Desmidiaceae of the European Lowlands.* KNNV Publishing, Zeist, The Netherlands, 351 pp.

Compère, P. 1977. *Staurodesmus* Teiling (Desmidiacées). Typification du genre et combinations nouvelles. *Bull. Jard. Bot. Nat. Belg.* 47:262–4.

Denboh, T., Ichimura, T., Hendrayanti, D. & Coleman, A. D. 2003. *Closterium moniliferum-ehrenbergii* (Charophyceae, Chlorophyta) species complex viewed from the 1506 group I intron and ITS2 of nuclear rDNA. *J. Phycol.* 39:960–77.

Förster, K. 1983. Revision und Validierung von Desmidiaceen-Namen aus früheren Publikationen. 3. *Algol. Studies* 33:375–87.

Gay, F. 1884. Note sur les Conjugées du midi de la France. *Bull Soc. Bot. France* 31:331–42.

Gontcharov, A. A. 2008. Phylogeny and classification of Zygnematophyceae (Streptophyta): current state of affairs. *Fottea* 8:87–104.

Gontcharov, A. A., Finlay, D. L., Kling, H. J. & Watanabe, M. M. 2002. Desmids (Desmidiales, Streptophyta) from the Experimental Lakes Area, Ontario, Canada. The genera *Actinotaenium* and *Cosmarium. Algol. Studies* 106:17–41.

Gontcharov, A. A., Marin, B. & Melkonian, M. 2003. Molecular phylogeny of conjugating green algae (*Zygnemophyceae, Streptophyta*) inferred from SSU rDNA sequence comparisons. *J. Mol. Evol.* 56:89–104.

Gontcharov, A. A. & Melkonian, M. 2005. Molecular phylogeny of *Staurastrum* Meyen ex Ralfs and related genera (Zygnematophyceae, Streptophyta) based on coding and noncoding rDNA sequence comparisons. *J. Phycol.* 41:887–99.

Gontcharov, A. A. & Melkonian, M. 2008. In search of monophyletic taxa in the family Desmidiaceae (Zygnematophyceae, Viridiplantae): the genus *Cosmarium. Am. J. Bot.* 95:1079–95.

Gontcharov, A. A. & Melkonian, M. 2010. Molecular phylogeny and revision of the genus *Netrium* (Zygnematophyceae, Streptophyta): *Nucleotaenium* gen. nov. *J. Phycol.* 46:346–62.

Gontcharov, A. A. & Melkonian, M. 2011. A study of conflict between molecular phylogeny and taxonomy in the Desmidiaceae (Streptophyta, Viridiplantae): analyses of 291 *rbc*L sequences. *Protist* 162:253–67.

Grönblad, R. 1921. New desmids from Finland and northern Russia with critical remarks on some known species. *Acta Soc. Fauna Fl. Fenn.* 49:1–78.

Guiry, M. D. & Guiry, G. M. 2012. *AlgaeBase.* World-wide electronic publication, National University of Ireland, Galway. Available at: http://www.algaebase.org.

Hall, J. D., Fučíková, K., Lo, C., Lewis, L. A. & Karol, K. G. 2010. An assessment of proposed DNA barcodes in freshwater green algae. *Cryptogam. Algol.* 31:529–55.

Hall, J. D., Karol, K. G., McCourt, R. M. & Delwiche, C. F. 2008. Phylogeny of the conjugating green algae based on chloroplast and mitochondrial nucleotide sequence data. *J. Phycol.* 44:467–77.

Hammer, O., Harper, D. A. T. & Ryan, P. D. 2001. PAST: palaeontological Statistics software package for education and data analysis. *Paleontol. Electron.* 4:1–9.

Höftberger, M. & Meindl, U. 1993. Cell differentiation, ultrastructure and nuclear migration in the desmid *Xanthidium armatum. Nova Hedwig.* 56:75–88.

Hepperle, D. 2004. *SeqAssem©.* A sequence analysis tool, contig assembler and trace data visualization tool for molecular sequences. Available at: http://www.sequentix.de.

Irénée-Marie, F. 1939. *Flore desmidiale de la Région de Montréal.* La Prairie, Canada, 547 pp.

Klingenberg, C. P., Barluenga, M. & Meyer, A. 2002. Shape analysis of symmetric structures: quantifying variation among individuals and asymmetry. *Evolution* 56:1909–20.

Kouwets, F. A. C. 1999. *A Check - list of Desmids (Chlorophyta, Zygnemaphyceae) of France.* Service du Patrimoine Naturel, Paris, 150 pp.

Kouwets, F. A. C. 2008. The species concepts in desmids: the problem of variability, infraspecific taxa and the monothetic species definition. *Biologia* 63:877–83.

Krasznai, E., Feher, G., Borics, G., Varbiro, G., Grigorszky, I. & Tothmeresz, B. 2008. Use of desmids to assess the natural conservation value of a Hungarian oxbow (Malom-Tisza, NE-Hungary. *Biologia* 63:928–35.

Kumar, S., Dudley, J., Nei, M. & Tamura, K. 2008. MEGA: a biologist-centric software for evolutionary analysis of DNA and protein sequences. *Brief. Bioinform.* 9:299–306.

Lagerheim, G. 1888. Über Desmidiaceen aus Bengalen nebst Bemerkungen über die geographische Verbreitung der Desmidiaceen in Asien. *Bih. Kongl. Svensk. Vet.-Akad. Handl.* 13 (Afd. III, 9):1–12

Lenzenweger, R. 1997. Desmidiaceenflora von Österreich, Teil 2. *In* Cramer, J. [Ed.] *Bibliotheca Phycologica 102.* Gebrüder Borntraeger Verlagsbuchhandlung, Berlin-Stuttgart, pp. 1–216.

Lowe, C. W. 1923. *Report of the Canadian Arctic Expedition 1913–1918. Vol. 4. Botany, Part A. Freshwater Algae and Diatoms.* F. A. Acland, Ottawa, 53 pp.

Lundell, P. M. 1871. De Desmidiaceis quae in Suecia inventae sunt, observationes criticae. *Nova Acta Reg. Soc. Sci. Upsal. III* 8:1–100.

McCourt, R. M., Karol, K. G., Bell, J., Helm-Bychowski, K. M., Grajewska, A., Wojciechowski, M. F. & Hoshaw, R. W. 2000. Phylogeny of the conjugating green algae (Zygnemophyceae) based on rbcL sequences. *J. Phycol.* 36:747–58.

McNeill, J., Barrie, F. R., Burdet, H. M., Demoulin, V., Hawksworth, D. L., Marhold, K., Nicolson, D. H. et al. 2006. International code of botanical nomenclature (Vienna code). *Regn. Veg.* 146:1–568.

Meindl, U. 1986. Autonomous circular and radial motions of the nucleus in *Pleurenterium tumidum* and their relation to cytoskeletal elements and the plasma membrane. *Protoplasma* 135:50–66.

Moore, W. S. 1995. Inferring phylogenies from mtDNA variation – Mitochondrial gene trees versus nuclear-gene trees. *Evolution* 49:718–26.

Nemjová, K., Neustupa, J., Šťastný, J., Škaloud, P. & Veselá, J. 2011. Species concept and morphological differentiation of strains traditionally assigned to *Micrasterias truncata*. *Phycol. Res.* 59:208–20.

Neustupa, J., Černá, K. & Šťastný, J. 2009. Diversity and morphological disparity of desmid assemblages in Central European peatlands. *Hydrobiologia* 630:243–56.

Neustupa, J., Černá, K. & Šťastný, J. 2011a. The effect of aperiodic desiccation on the diversity of benthic desmid assemblages in a lowland peat bog. *Biodiv. Conserv.* 20:1695–711.

Neustupa, J., Škaloud, P. & Šťastný, J. 2010. The molecular phylogenetic and geometric morphometric evaluation of *Micrasterias crux-melitensis/M. radians* species complex. *J. Phycol.* 46:703–14.

Neustupa, J. & Šťastný, J. 2006. The geometric morphometric study of Central European species of the genus *Micrasterias* (Zygnematophyceae, Viridiplantae). *Preslia* 78:253–63.

Neustupa, J., Šťastný, J., Nemjová, K., Mazalová, P., Goodyer, E., Poulíčková, A. & Škaloud, P. 2011b. A novel, combined approach to assessing species delimitation and biogeography within the well-known desmid species *Micrasterias fimbriata* and *M. rotata* (Desmidiales, Steptophyta). *Hydrobiologia* 667:223–39.

Nylander, J. A. A. 2004. *MrModeltest v2*. Evolutionary Biology Centre, Uppsala University, Uppsala, Sweden. Available at http://www.abc.se/~nylander.

Pals, A., Elst, D., Muylaert, K. & Van Assche, J. 2006. Substrate specificity of periphytic desmids in shallow softwater lakes in Belgium. *Hydrobiologia* 568:159–68.

Pamilo, P. & Nei, M. 1988. Relationships between gene trees and species trees. *Mol. Biol. Evol.* 5:568–83.

Potapova, M. & Hamilton, P. B. 2007. Morphological and ecological variation within the *Achnanthidium minutissimum* (Bacillariophyceae) species complex. *J. Phycol.* 43:561–75.

Prescott, G. W., Bicudo, C. E. M. & Vinyard, W. C. 1982. *A Synopsis of North American Desmids. Part II. Desmidiaceae: Placodermae, Section 4*. University of Nebraska Press, Lincoln and London, 700 pp.

Pritchard, A. 1861. *A History of Infusoria, Living and Fossil: Arranged According to Die Infusionsthierchen of C.G. Ehrenberg; Containing Colored Engravings, Illustrative of all the Genera, and Descriptions of all the Species in that Work, with Several New Ones*. Whittaker and Co., London, 968 pp.

Ralfs, J. 1848. *The British Desmidieae*. Reeve, Benham and Reeve, London, 226 pp.

Rich, S. M., Rosenthal, B. M., Telford, S. R. III, Spielman, A., Hartl, D. L. & Ayala, F. J. 1997. Heterogeneity of the internal transcribed spacer (ITS-2) region within individual deer ticks. *Insect Mol. Biol.* 6:123–9.

Ronquist, F. & Huelsenbeck, J. P. 2003. MRBAYES 3: bayesian phylogenetic inference under mixed models. *Bioinformatics* 19:1572–4.

Rosenberg, N. A. 2003. The shapes of neutral gene genealogies in two species: probabilities of monophyly, paraphyly, and polyphyly in a coalescent model. *Evolution* 61:225–47.

Shaw, J., Lickey, E. B., Beck, J. T., Farmer, S. B., Liu, W., Miller, J., Siripun, K. C., Winder, C. T., Schilling, E. E. & Small, R. L. 2005. The tortoise and the hare II: relative utility of 21 noncoding chloroplast DNA sequences for phylogenetic analysis. *Am. J. Bot.* 92:142–66.

Škaloud, P., Nemjová, K., Veselá, J., Černá, K. & Neustupa, J. 2011. A multilocus phylogeny of the desmid genus *Micrasterias* (Streptophyta): evidence for the accelerated rate of molecular evolution in protists. *Mol. Phylog. Evol.* 61:933–43.

Škaloud, P., Šťastný, J., Nemjová, K., Mazalová, P. & Neustupa, J. 2012. Molecular phylogeny of baculiform desmid taxa. *Plant Syst. Evol.* 298:1281–92.

Šťastný, J. 2010. Desmids (Conjugatophyceae, Viridiplantae) from the Czech Republic; new and rare taxa, distribution, ecology. *Fottea* 10:1–74.

Swofford, D.L. 2002. *PAUP*. Phylogenetic Analysis Using Parsimony (* and other methods). Version 4*. Sinauer Associates, Sunderland, Massachusetts, 142 pp.

White, T. J., Bruns, T., Lee, S. & Taylor, J. W. 1990. Amplification and direct sequencing of fungal ribosomal RNA genes for phylogenetics. *In* Innis, M. A., Gelfand, D. H., Sninsky, J. J. & White, T. J. [Eds.] *PCR Protocols: A Guide to Methods and Applications*. Academic Press, New York, pp. 315–22.

Teiling, E. 1956. On the variation of *Micrasterias mahabuleshwarensis* f. *Wallichii*. *Bot. Not.* 109:260–74.

Verbruggen, H., Maggs, C. A., Saunders, G. W., Le Gall, L., Yoon, H. S. & De Clerck, O. 2010. Data mining approach identifies research priorities and data requirements for resolving the red algal tree of life. *BMC Evol. Biol.* 10:1–16.

Veselá, J., Neustupa, J., Pichrtová, M. & Poulíčková, A. 2009. Morphometric study of *Navicula* morphospecies (Bacillariophyta) with respect to diatom life cycle. *Fottea* 9:307–16.

West, W. & West, G. S. 1912. *A Monograph of the British Desmidiaceae, Vol IV*. The Ray Society, London, 194 pp.

White, T. J., Bruns, T., Lee, S. & Taylor, J. W. 1990. Amplification and direct sequencing of fungal ribosomal RNA genes for phylogenetics. *In* Innis, M. A., Gelfand, D. H., Sninsky, J. J. & White, T. J. [Eds.] *PCR Protocols: A Guide to Methods and Applications*. Academic Press, New York, pp. 315–22.

Wille, N. 1890. Desmidiaceae. *In* Engler & Prantl (Eds.) *Die natürlichen Pflanzenfamilien*, I, 2. Leipzig, Germany, pp. 1–175.

Williamson, D. B. 2002. Rare desmids from garden ornaments and Scottish lochs. *Algol. Studies* 105:79–86.

Zelditch, M. L., Swiderski, D. L., Sheets, H. D. & Fink, W. L. 2004. *Geometric Morphometrics for Biologists. A Primer*. Elsevier Academic Press, London, 443 pp.

Zuker, M. 2003. Mfold web server for nucleic acid folding and hybridization prediction. *Nucleic Acids Res.* 31:3406–15.

Zwickl, D. J. 2009. Phylogenetic analysis of molecular sequnce data using the maximum-likelihood criterion. Available at: http://code.google.com/p/garli/.

Supporting Information

Additional Supporting Information may be found in the online version of this article at the publisher's web site:

Table S1. List of all sequences involved in the phylogenetic analyses, including the GenBank accession numbers for the *rbc*L, *cox*III, *trn*G^{ucc}, and ITS rDNA genes. Strain number abbreviations: ACOI - Coimbra Collection of Algae, Portugal; ACKU - Algal Culture Collection of Kyonggi University, Kyonggi, Korea; CCAP - Culture Collection of Algae and Protozoa, Oban, Scotland, UK; JH - John Hall private collection; M - Culture Collection Melkonian, University of Cologne, Germany (strains available from CCAC); NIES - National Institute for Environmental Studies, Japan; SAG - Sammlung von Algenkulturen der Universität Göttingen, Germany; SVCK - Sammlung von Conjugaten-Kulturen, Germany; UTEX - Culture Collection of Algae at University of Texas, USA.

Appendix S1. LM and SEM pictures of all the *Xanthidium* strains studied.